Identifying Discrepancies in HIV Infectivity and Virion Maturation Using FRET-Based Detection and Quantification

Kedhar Narayan[1†], Jeongpill Choi[1†], Shreyas S. Gujar[1†], Aidan McGraw[1†], Hasset Tibebe[1], Lilia Mei Bose[1], Caroline N. Arnette[1], Taisuke Izumi[1, 2*]

[1]Department of Biology, College of Arts and Sciences, American University, Washington D.C., USA

[2] District of Columbia Center for AIDS Research, Washington D.C., USA

[†]These authors contributed equally to this work

*Author to whom correspondence should be addressed

Abstract

The maturation of HIV-1 virions is a crucial process in viral replication. Although T cells are a primary source of virus production, much of our understanding of virion maturation comes from studies using the HEK293T human embryonic kidney cell line. Notably, there is a lack of comparative analyses between T cells and HEK293T cells in terms of virion maturation efficiency in existing literature. We previously developed an advanced virion visualization system based on the FRET principle, enabling the effective distinction between immature and mature virions via fluorescence microscopy. In this study, fully infectious FRET-labeled viruses (HIV-1 Gag-iFRET) from Jurkat (a human T lymphocyte cell line) and HEK293T cells were used to assess their virion maturation rates. Our results showed that viruses originating from Jurkat cells had an infectivity rate approximately tenfold higher than that from HEK293T cells. Concerning virion maturity, HEK293T-derived virions demonstrated a maturity rate of 81.79%, consistent with other studies and our previous findings. However, virions from Jurkat cells exhibited a notably lower maturity rate of 68.67% ($p < 0.0001$), indicating an interesting deviation from the expected positive correlation with infectivity. These findings suggest that the initiation of virion maturation does not directly correlate with viral infectivity. Instead, these observations suggest that the rate of conical core formation following the initiation of virion maturation plays a more pivotal role in determining viral infectivity, even when the overall level of maturation is relatively low.

Keywords:

Human Immunodeficiency Virus (HIV), Forster Resonance Energy Transfer (FRET), Virion Maturation, Comparative Viral Analysis, Fluorescent Microscopic Imaging,

1. Introduction

Human Immunodeficiency Virus-1 (HIV-1) continues to pose a significant global health challenge. The advancement of combination antivirals has dramatically improved the management of HIV, targeting various stages of the virus lifecycle, including entry, reverse transcription, integration, and protease activity [1-6]. Recently, the development of capsid inhibitors has emerged as a promising strategy for long-acting antiviral treatments against HIV-1 [7-12]. These novel inhibitors, targeting critical steps in both the early and late stages of the virus lifecycle, notably disrupt the formation of infectious particles. This innovation underscores the need for a comprehensive understanding of the virion maturation process, a key phase in the HIV life cycle where non-infectious particles are transformed into infectious virions.

Our previous research developed a unique tool for detecting virus maturation utilizing a fluorescence resonance energy transfer (FRET)-based technique [13]. This approach enables the semi-automatic evaluation of virion maturation through fluorescent microscopy, effectively minimizing human bias. It offers crucial insights into the structural changes that are vital for virus infectivity. Building upon this, our current study explores virion maturation in different cellular environments. Although T cells are recognized as the primary site for HIV-1 replication [14-20], most existing research assessing viral maturation predominantly utilizes the HEK293T human embryonic kidney cell line [21-24]. Utilizing the FRET-based system, we generated infectious FRET-labeled viruses in both HEK293T and Jurkat cells, an immortal human T-cell leukemia cell line. Surprisingly, we observed that viruses produced by Jurkat cells exhibited a significantly lower maturation efficiency (approximately 69%) compared to those from HEK293T cells (approximately 82%). Contrasting with this, the infectivity of viruses from Jurkat cells was around ten times higher than those

from HEK293T cells. These findings call into question the previously accepted belief of a direct correlation between virion maturation and virus infectivity, thereby deepening our understanding of the intricate balance between these two crucial aspects, virion maturation and virus infectivity of HIV-1 pathology. This research represents the first to specifically compare the virion maturation in different cell lines.

2. Materials and Methods

2.1 Plasmid DNA Construction

The plasmid DNA utilized for HIV-1 Gag-iFRET labeling virus production incorporates an efficient intramolecular FRET pair, ECFPΔC11 and cp173Venus [25]. These genes are positioned between the MA and CA regions of the HIV-1 Gag protein based on the HIV-1 Gag-iGFP construct [26]. The FRET pair genes, along with the junction with the MA and CA regions, are flanked by HIV-1 protease cleavage sites (SQNYPIVQ). This design enables the HIV-1 Protease to specifically cleave at these sites, resulting in a modification of the FRET signal during the maturation of the virion. Additional details are provided in our previous publication [13].

2.2 Virus Production and Cell Culture

HIV-1 Gag-iFRET plasmid DNA was transfected into HEK293T cells using a PEI transfection method (Polysciences) and into Jurkat cells using the Neon NxT Electroporation System (Invitrogen). HEK293T and TZM-bl cells were cultured in Dulbecco's Modified Eagle's Medium (Cytiva) supplemented with 10% Fetal Bovine Serum (Gibco), 1% Penicillin-Streptomycin-Glutamine (Invitrogen), and 1%

87 GlutaMax (Gibco)(D10) at 37°C in a 5% CO2 environment. Suspended Jurkat cells
88 were cultured in RPMI 1640 media (Cytiva) with the same supplements (R10). For
89 producing FRET-labelled virions, HEK293T cells (3.5×10^6 cells/10 cm dish) or
90 Jurkat cells (2×10^6 cells/24 well plate) were co-transfected with pHIV-1 Gag-iFRET
91 or iFRETΔPro and the parental plasmid pNL4-3 or pNL43ΔPro at a 1:10 ratio. Post-
92 transfection, the culture medium was replaced with fresh D10 medium after 3.5
93 hours for PEI transfection. Virus-containing supernatants were collected 24 hours
94 post-medium change from HEK293T cells or 72 hours post-electroporation from
95 Jurkat cells. The supernatants were then filtered through a 0.45 μm sterile
96 polyvinylidene difluoride (PVDF, Millipore) membrane and concentrated up to 20-fold
97 using Lenti-X Concentrator (TaKaRa). Finally, the virus pellet was resuspended in
98 500 μL of Hank's Balanced Salt Solution (HBSS) without phenol red (Cytiva).

99

100 2.3 FRET-Based Virion Visualization

101 To visualize HIV-1 Gag-iFRET/iFRETΔPro labeled virions, the concentrated virus
102 supernatant was diluted 800-fold in 0.22 μm PVDF filtered Hank's Balanced Salt
103 Solution (HBSS) without Phenol Red (Cytiva) and loaded (350 μL) onto non-coated
104 30mm x 10mm glass-bottom Tissue Culture Treated Dish (CELLTREAT). The Dish
105 was then incubated overnight at 4°C. Single-virion images were captured using an
106 A1R MP+ Multiphoton Confocal Microscope (Nikon). Two sets of 21 images were
107 automatically acquired for each sample under optimal focus conditions. The first set
108 employed a 457.9 nm laser for CFP excitation, capturing emissions through 482
109 nm/35 nm and 540 nm/30 nm filter cubes for CFP and YFP signals, respectively
110 (FRET images). The second set used a 514.5 nm laser for Venus excitation, with

111 emissions read through a 540 nm/30 nm filter cube to detect the YFP signal. The
112 maturation status was quantified as FRET efficiency relative to signals detected in
113 HIV-1 Gag-iFRETΔ1Pro labeled virions. Images were captured in RAW ND2 format
114 and converted to TIFF files using Fiji, an image processing package based on
115 ImageJ2. Binary images, generated based on the YFP signal, provided XY
116 coordinates for each particle. Using these coordinates, the FRET signal intensity of
117 each virion was extracted from the raw data, and the FRET ratio (YFP/CFP) was
118 calculated for each particle. Histograms displaying the distribution of FRET ratio
119 values were generated, with 100 bins division, and kernel density estimation curves
120 were plotted alongside. The proportion of the total Gaussian distribution or kernel
121 density estimation area overlapping with the HIV-1 Gag-iFRETΔPro area was used
122 to determine the proportion of immature virions. Image data analysis and subsequent
123 calculations of mature and immature virion proportions were performed using an
124 updated in-house MATLAB program [13].

125

126 2.4 Infectivity Assays

127 Pseudotyped parental NL4-3 viruses were produced in HEK293T or Jurkat cells
128 using the transfection methods described in the above FRET-based Virion
129 Visualization section. The cells were transfected with pNL4-3ΔEnv parental plasmid
130 along with the HIV-1 envelope expression plasmid pSVIII-92HT593.1, kindly
131 provided by Dr. Viviana Simon at Mount Sinai. Viral titers were determined using the
132 HIV-1 Gag p24 DuoSet ELISA (R&D Systems). After seeding TZM-bl cells at 5×10^3
133 in 96-well plates, they were exposed to an equivalent amount of virus (5 ng of HIV-1
134 p24 total) the following day. The cells were incubated at 37°C for 48 hours in a CO^2

135 incubator. Subsequently, luciferase activity in the infected cells was measured with
136 the Luciferase Assay System (Promega) using a Molecular Devices SpectraMax
137 Microplate Reader.

138

139 2.5 Statistical Analysis

140 Data were analyzed using standard statistical methods. The significance of
141 differences in virion maturation and infectivity between the two cell types was
142 determined using the Mann-Whitney U test and an unpaired *t*-test with Welch's
143 correction, respectively, with a p-value of less than 0.05 considered statistically
144 significant.

145

146 **3. Results**

147 3.1 Virion Maturation Efficiency in Different Producer Cells

148 In this study, we quantified the proportion of mature and immature virions in FRET-
149 labeled viruses produced by HEK293T (kidney cell lines) and Jurkat (T-cell leukemia
150 cell lines). In each sample, we captured a total of 21 images, from which we created
151 binary images based on the emitted and excited images of YFP (Fig. 1A). We then
152 calculated the FRET ratio for each virion by dividing the intensity of YFP (the FRET
153 acceptor) by the total CFP intensity, which serves as the FRET donor. After
154 calculating the FRET ratio for each virion, based on the extracted signal intensities of
155 the FRET donor and acceptor, we applied kernel density estimation to the
156 histograms of FRET efficiencies. The area where the HIV-1 Gag-iFRET curve
157 overlapped with the HIV-1 Gag-iFRETΔPro curve was identified as the proportion of

158 immature virions, as per our established methodology (Fig. 1B) [13]. In our analysis,
159 we examined 14,021 and 22,779 particles, as well as 20,457 and 23,181 particles of
160 HIV-1 Gag-iFRET and HIV-1 Gag-iFRETΔPro labeled virions produced by HEK293T
161 and Jurkat cells, respectively, across three independent experiments. The mature
162 virion proportion in the HIV-1 Gag-iFRET population from HEK293T cells was
163 81.79% ± 0.06 (Fig. 1C), consistent with our previous findings and electron
164 microscopic counts reported in other studies [13, 21-24]. In contrast, Jurkat cells
165 produced mature virions at a lower rate of 68.67% ± 0.04 (Fig. 1C), which is
166 significantly different from that of HEK293T cells (p-value < 0.0001). Furthermore, we
167 quantified the Mean Fluorescent Intensity (MFI) of the YFP signal in both mature and
168 immature virions. The results confirmed that the average incorporation of fluorescent
169 proteins, indicated by the MFI of YFP (Fig. 1D), was similar in both mature and
170 immature virions from HEK293T and Jurkat cells (26,691.31 ± 2,733.73 vs.
171 23,309.51 ± 766.93 in mature virions and 24,619.37 ± 2,857.71 vs. 24,536.10 ±
172 2,046.71 in immature virions, respectively, and 24,619.37 ± 2,857.71 vs. 24,536.10 ±
173 2,036.70 in ΔPro). These findings indicate that the number of incorporated
174 fluorescent proteins is comparable, ensuring that the FRET energy transfer efficiency
175 is neither under nor overestimated in virions produced by either HEK293T or Jurkat
176 cells.

177

178 3.2 Virus Infectivity in Different Producer Cells

179 To further examine the characteristic differences between viruses produced by
180 HEK293T and Jurkat cells, we performed a single-round infection assay using TZM-
181 bl cells to assess the infectivity of FRET-labeled viruses originating from these cell

182 lines. Notably, viruses produced in Jurkat cells exhibited relative infectivity
183 approximately tenfold higher than those from HEK293T cells (Fig. 2). This marked
184 difference in infectivity was consistently observed in three independent experiments.

185

186 **4.1 Discussion**

187 The findings of this study provide groundbreaking insights into the maturation
188 process of HIV-1 virions and its impact on viral infectivity, challenging several
189 established notions in the field. Our utilization of an advanced FRET-based
190 visualization system has allowed for a detailed comparative analysis of virion
191 maturation in two distinct cellular environments, HEK293T and Jurkat cell lines. One
192 of the most striking observations from our research is the inverse relationship
193 between virion maturation efficiency and infectivity. While HEK293T cells exhibited a
194 higher rate of virion maturation (81.79%), virions from Jurkat cells, with a lower
195 maturation rate of 68.67%, demonstrated significantly higher infectivity,
196 approximately tenfold greater than the HEK293T counterparts. This finding is in stark
197 contrast to the traditional view that higher virion maturation correlates directly with
198 increased infectivity. It suggests that factors other than maturation efficiency, possibly
199 inherent to the host cell environment or the virion composition, play a crucial role in
200 determining the infectivity of HIV-1. Recent studies have provided deeper insights
201 into the role of Inositol hexakisphosphate (IP6) in HIV-1 capsid assembly, a critical
202 factor in virus infectivity [27]. These studies reveal that the immature Gag lattice of
203 HIV-1 virions enriches IP6, facilitating capsid maturation. This process is
204 characterized by the proteolysis of the Gag polyprotein by the viral protease,
205 inducing vital conformational changes in the capsid protein (CA). These changes

206 lead to the formation of a conical, cone-shaped mature capsid, consisting of over
207 1,000 CA copies and forming approximately 200 hexamers and 12 pentamers,
208 known collectively as capsomers. In the context of our FRET-based assay, which
209 specifically detects the cleavage of the Gag polyprotein between MA-CA, research
210 by Sowd et al. has shown that IP6-depleted T-cell lines produce virion particles with
211 incompletely cleaved Gag proteins [28]. This study indicated that virions from IP6-
212 deficient cells exhibited lower quantities of mature MA and CA cleavage products
213 and higher proportions of MA-CA-SP1/MA-CA cleavage intermediates compared to
214 virions from wild-type cells. Therefore, our FRET detection system could potentially
215 monitor the IP6-dependent efficiency of Gag polyprotein cleavage. Furthermore, they
216 characterized virus particle morphology using electron microscopy and calculated
217 that mature conical core particles in another T-cell leukemia cell line, MT-4 cells,
218 comprised 62% of the total virion, which aligns with the result from our FRET
219 detection system in Jurkat cells (Fig. 1B [II] and 1C).

220 Another study employing a similar concept of FRET-based assay with different FRET
221 pair proteins reveals that the activation of the HIV-1 viral protease occurs during
222 assembly and budding before the release of particles in HEK293T cells [29]. Since
223 the recruitment of IP6 requires the immature Gag lattice, understanding the extent of
224 viral protease activation during assembly and its role in initiating Gag polyprotein
225 cleavage before particle release must be crucial. This early activation potentially
226 influences the formation of the infectious core through IP6 recruitment. Our results,
227 combined with previous reports, lead to the hypothesis that virions produced by
228 HEK293T cells may undergo partial Gag-polyprotein cleavage prior to release from
229 the assembly site. Moreover, several researchers have shown by electron
230 microscopic analyses that about 70% of viruses produced by HEK293T cells contain

closed conical cores, while the remaining 30% display eccentric or aberrant forms among the mature virions [21-23]. This suggests that only around 56% of total virions from HEK293T cells have a closed conical core, a proportion likely lower than that observed in viruses produced by T-cell lines, which is about 62% [28]. The early maturation observed in HEK293T cells may result in decreased recruitment of IP6 within the virions, which could affect the formation of the infectious conical core. This phenomenon likely contributes to the higher maturation ratio observed in HEK293T cells in our study and in other research (Fig. 1) [29]. However, this early maturation might also lead to a reduction in viral infectivity when compared to virions produced in Jurkat cells (Fig. 2). Mathematical modeling suggests that the transport of the pre-integration complex into the nucleus, along with DNA integration and reverse transcription, is one of the major factors that significantly influence HIV-1 replication [30]. The formation of a conical core is essential for both steps of reverse transcription and the subsequent transport of viral DNA into the nucleus for integration into the host genome [31, 32]. Consequently, the formation of an infectious conical core following Gag polyprotein cleavage is a critical determinant of virus infectivity. This implies that viruses produced from T-cell lines may be more efficient in forming appropriate conical cores, thereby enhancing their infectivity.

Our research fills a crucial gap in the existing literature by providing a comparative analysis of virion maturation in kidney cells (HEK293T) and T cells (Jurkat). This comparison is vital, considering T cells are the primary source of HIV-1 replication *in vivo*. The observed differences in maturation efficiencies and infectivity rates between HEK293T and Jurkat cells highlight the importance of considering the cellular context in HIV-1 biology and pathogenesis studies. Furthermore, our findings have significant implications for the evaluation of antiviral effects, particularly in the

256 context of long-acting treatments with maturation and capsid inhibitors. These
257 inhibitors target various stages of virus infection, including viral budding and virion
258 maturation [33-35]. The substantial disparities in viral maturation rates between T-
259 cells and HEK293T cells, the latter of which is a standard cellular resource for *in-vitro*
260 virus production, suggest that relying solely on HEK293T cells could lead to
261 misleading assessments of antiviral efficacy. Therefore, our study indicates the
262 necessity of including T-cell-based assessments to more accurately determine the
263 antiviral efficacy of maturation and capsid inhibitors in virus maturation. In addition,
264 by pinpointing the stages at which these inhibitors can be most effective, our findings
265 could contribute to more efficient and effective HIV treatment regimens.

266 In conclusion, the results of our study not only enhance our understanding of HIV-1
267 pathogenesis but also emphasize the complexity of the virus life cycle. The unique
268 insights gained into the relationship between virion maturation and infectivity open
269 new pathways for future research, potentially leading to novel therapeutic
270 approaches in the fight against HIV.

271

272 **Author's contributions**

273 TI conceptualized and designed the study. Experiments were carried out by JC, AM,
274 SG, HT, LMB, CA, and TI. The development of the in-house MATLAB script for
275 automated image data analysis was a collaborative effort between KN and TI. Data
276 analysis was conducted by KN, SG, and TI. The manuscript was written by TI. TI
277 provides financial support for the research. All authors have made substantial
278 contributions to the work and have given their approval for the final version of the
279 article to be published.

Funding

This study is partially supported by a research start-up fund from American University (Grant Number: 75316 to TI). Additional funding was provided by the National Institutes of Health, specifically through a grant from the National Institute of Allergy and Infectious Diseases (Grant Number: 7R15AI172610-02 to TI).

Acknowledgments

We extend our thanks to Dr. Viviana Simon at Mount Sinai for generously providing the pSVIII-92HT593.1 plasmid DNA.

Figure Legend

Figure 1. Quantitative Analysis of Mature Virions from HEK293T and Jurkat Cells.

(A) Representative FRET-labeled HIV-1 Gag-iFRET virion images from Jurkat cells displayed in a single field. The left panel shows an image captured through the YFP excitation (515 nm) and emission (540 nm) channels (YFP channel). The second image shows the binary image, derived from the YFP channel, identifying virus particle locations as regions of interest (ROI). The third and fourth images are captured using CFP (FRET donor) excitation (454 nm), with CFP emission (483 nm, third) and YFP emission (540 nm, fourth) channels. The right panel shows the FRET efficiency ratio view, computationally constructed from FRET donor (CFP excitation/CFP emission) and acceptor (CFP excitation/YFP emission) images. The

303 color spectrum indicates FRET signal strength, with high FRET appearing in red
304 (yellow arrows) and decreasing FRET shifting toward blue (white arrows). (B) Kernel
305 Density Estimation Curves of FRET Intensity in HIV-1 Gag-iFRET Virions Produced
306 by HEK293T and Jurkat Cells. The curves depict the distribution histograms of FRET
307 intensity for virions labeled with HIV-1 Gag-iFRET from (I) HEK293T and (II) Jurkat
308 cells. The x-axis represents the range of FRET intensity. The y-axis shows the
309 adjusted density of curves for both HIV-1 Gag-iFRET and HIV-1 Gag-iFRET∆Pro
310 virions. The area under the curve for HIV-1 Gag-iFRET overlapping with that of HIV-1
311 Gag-iFRET∆Pro is calculated and considered indicative of the proportion of
312 immature virions within the total population of HIV-1 Gag-iFRET virions. (C) Scatter
313 Plot of Mature Virion Quantification displays the median percentage of mature virions
314 across 21 images derived from three independent experiments, culminating in a total
315 of 63 data points. Statistical significance was assessed using the Mann-Whitney U
316 test. (D) Comparison of Mean Fluorescent Intensity (MFI) of YFP Signals in Mature
317 and Immature HIV-1 Gag-iFRET labeling Virions. The levels of fluorescent protein
318 incorporation, as indicated by the YFP signal, were not significantly different between
319 mature and immature virions in either the wild-type or ∆Pro viruses. The error bars
320 represent the standard error from three independent experiments. Statistical
321 significance was assessed using the Wilcoxon matched-pairs signed rank test.

322

323 **Figure 2. Comparing Virus Infectivity Between HEK293T and Jurkat Cells**.

324 Single-round infectivity assays using TZM-bl cells were performed to evaluate the
325 differences in virus infectivity produced by HEK293T and Jurkat cells. The bar plot
326 illustrates the relative infectivity (%) of the NL4-3 virus produced by Jurkat cells in

327 comparison to its infectivity when produced by HEK293T cells. Error bars represent
328 the standard deviation from three independent experiments. Statistical significance
329 was determined using an unpaired *t*-test with Welch's correction.

330

331 **References**

332 1. Ghosh, A. K., Four decades of continuing innovations in the development of
333 antiretroviral therapy for HIV/AIDS: Progress to date and future challenges.
334 *Glob Health Med* **2023,** 5, (4), 194-198.
335 2. Landovitz, R. J.; Scott, H.; Deeks, S. G., Prevention, treatment and cure of
336 HIV infection. *Nat Rev Microbiol* **2023,** 21, (10), 657-670.
337 3. Arts, E. J.; Hazuda, D. J., HIV-1 antiretroviral drug therapy. *Cold Spring Harb*
338 *Perspect Med* **2012,** 2, (4), a007161.
339 4. Magden, J.; Kaariainen, L.; Ahola, T., Inhibitors of virus replication: recent
340 developments and prospects. *Appl Microbiol Biotechnol* **2005,** 66, (6), 612-21.
341 5. Adamson, C. S.; Freed, E. O., Novel approaches to inhibiting HIV-1
342 replication. *Antiviral Res* **2010,** 85, (1), 119-41.
343 6. Wiebe, L. I.; Knaus, E. E., Concepts for the design of anti-HIV nucleoside
344 prodrugs for treating cephalic HIV infection. *Adv Drug Deliv Rev* **1999,** 39, (1-
345 3), 63-80.
346 7. Thenin-Houssier, S.; Valente, S. T., HIV-1 Capsid Inhibitors as Antiretroviral
347 Agents. *Curr HIV Res* **2016,** 14, (3), 270-82.
348 8. Yant, S. R.; Mulato, A.; Hansen, D.; Tse, W. C.; Niedziela-Majka, A.; Zhang, J.
349 R.; Stepan, G. J.; Jin, D.; Wong, M. H.; Perreira, J. M.; Singer, E.; Papalia, G.
350 A.; Hu, E. Y.; Zheng, J.; Lu, B.; Schroeder, S. D.; Chou, K.; Ahmadyar, S.;
351 Liclican, A.; Yu, H.; Novikov, N.; Paoli, E.; Gonik, D.; Ram, R. R.; Hung, M.;
352 McDougall, W. M.; Brass, A. L.; Sundquist, W. I.; Cihlar, T.; Link, J. O., A highly
353 potent long-acting small-molecule HIV-1 capsid inhibitor with efficacy in a
354 humanized mouse model. *Nat Med* **2019,** 25, (9), 1377-1384.

355 9. Singh, K.; Gallazzi, F.; Hill, K. J.; Burke, D. H.; Lange, M. J.; Quinn, T. P.;
356 Neogi, U.; Sonnerborg, A., GS-CA Compounds: First-In-Class HIV-1 Capsid
357 Inhibitors Covering Multiple Grounds. *Front Microbiol* **2019,** 10, 1227.
358 10. Sun, L.; Zhang, X.; Xu, S.; Huang, T.; Song, S.; Cherukupalli, S.; Zhan, P.; Liu,
359 X., An insight on medicinal aspects of novel HIV-1 capsid protein inhibitors.
360 *Eur J Med Chem* **2021,** 217, 113380.
361 11. Flexner, C.; Owen, A.; Siccardi, M.; Swindells, S., Long-acting drugs and
362 formulations for the treatment and prevention of HIV infection. *Int J Antimicrob*
363 *Agents* **2021,** 57, (1), 106220.
364 12. Gillis, E. P.; Parcella, K.; Bowsher, M.; Cook, J. H.; Iwuagwu, C.; Naidu, B. N.;
365 Patel, M.; Peese, K.; Huang, H.; Valera, L.; Wang, C.; Kieltyka, K.; Parker, D.
366 D.; Simmermacher, J.; Arnoult, E.; Nolte, R. T.; Wang, L.; Bender, J. A.;
367 Frennesson, D. B.; Saulnier, M.; Wang, A. X.; Meanwell, N. A.; Belema, M.;
368 Hanumegowda, U.; Jenkins, S.; Krystal, M.; Kadow, J. F.; Cockett, M.; Fridell,
369 R., Potent Long-Acting Inhibitors Targeting the HIV-1 Capsid Based on a
370 Versatile Quinazolin-4-one Scaffold. *J Med Chem* **2023,** 66, (3), 1941-1954.
371 13. Sarca, A. D.; Sardo, L.; Fukuda, H.; Matsui, H.; Shirakawa, K.; Horikawa, K.;
372 Takaori-Kondo, A.; Izumi, T., FRET-Based Detection and Quantification of
373 HIV-1 Virion Maturation. *Front Microbiol* **2021,** 12, 647452.
374 14. Chen, B., Molecular Mechanism of HIV-1 Entry. *Trends Microbiol* **2019,** 27,
375 (10), 878-891.
376 15. Pan, X.; Baldauf, H. M.; Keppler, O. T.; Fackler, O. T., Restrictions to HIV-1
377 replication in resting CD4+ T lymphocytes. *Cell Res* **2013,** 23, (7), 876-85.
378 16. Banga, R.; Procopio, F. A.; Noto, A.; Pollakis, G.; Cavassini, M.; Ohmiti, K.;
379 Corpataux, J. M.; de Leval, L.; Pantaleo, G.; Perreau, M., PD-1(+) and

380 follicular helper T cells are responsible for persistent HIV-1 transcription in
381 treated aviremic individuals. *Nat Med* **2016,** 22, (7), 754-61.
382 17. Berg, R. K.; Rahbek, S. H.; Kofod-Olsen, E.; Holm, C. K.; Melchjorsen, J.;
383 Jensen, D. G.; Hansen, A. L.; Jorgensen, L. B.; Ostergaard, L.; Tolstrup, M.;
384 Larsen, C. S.; Paludan, S. R.; Jakobsen, M. R.; Mogensen, T. H., T cells
385 detect intracellular DNA but fail to induce type I IFN responses: implications
386 for restriction of HIV replication. *PLoS One* **2014,** 9, (1), e84513.
387 18. Jones, R. B.; Ndhlovu, L. C.; Barbour, J. D.; Sheth, P. M.; Jha, A. R.; Long, B.
388 R.; Wong, J. C.; Satkunarajah, M.; Schweneker, M.; Chapman, J. M.; Gyenes,
389 G.; Vali, B.; Hyrcza, M. D.; Yue, F. Y.; Kovacs, C.; Sassi, A.; Loutfy, M.;
390 Halpenny, R.; Persad, D.; Spotts, G.; Hecht, F. M.; Chun, T. W.; McCune, J.
391 M.; Kaul, R.; Rini, J. M.; Nixon, D. F.; Ostrowski, M. A., Tim-3 expression
392 defines a novel population of dysfunctional T cells with highly elevated
393 frequencies in progressive HIV-1 infection. *J Exp Med* **2008,** 205, (12), 2763-
394 79.
395 19. Zhang, Z.; Schuler, T.; Zupancic, M.; Wietgrefe, S.; Staskus, K. A.; Reimann,
396 K. A.; Reinhart, T. A.; Rogan, M.; Cavert, W.; Miller, C. J.; Veazey, R. S.;
397 Notermans, D.; Little, S.; Danner, S. A.; Richman, D. D.; Havlir, D.; Wong, J.;
398 Jordan, H. L.; Schacker, T. W.; Racz, P.; Tenner-Racz, K.; Letvin, N. L.;
399 Wolinsky, S.; Haase, A. T., Sexual transmission and propagation of SIV and
400 HIV in resting and activated CD4+ T cells. *Science* **1999,** 286, (5443), 1353-7.
401 20. Groot, F.; van Capel, T. M.; Schuitemaker, J.; Berkhout, B.; de Jong, E. C.,
402 Differential susceptibility of naive, central memory and effector memory T cells
403 to dendritic cell-mediated HIV-1 transmission. *Retrovirology* **2006,** 3, 52.

404 21. Mattei, S.; Flemming, A.; Anders-Osswein, M.; Krausslich, H. G.; Briggs, J. A.;
405 Muller, B., RNA and Nucleocapsid Are Dispensable for Mature HIV-1 Capsid
406 Assembly. *J Virol* **2015,** 89, (19), 9739-47.
407 22. Keller, P. W.; Huang, R. K.; England, M. R.; Waki, K.; Cheng, N.; Heymann, J.
408 B.; Craven, R. C.; Freed, E. O.; Steven, A. C., A two-pronged structural
409 analysis of retroviral maturation indicates that core formation proceeds by a
410 disassembly-reassembly pathway rather than a displacive transition. *J Virol*
411 **2013,** 87, (24), 13655-64.
412 23. Fontana, J.; Jurado, K. A.; Cheng, N.; Ly, N. L.; Fuchs, J. R.; Gorelick, R. J.;
413 Engelman, A. N.; Steven, A. C., Distribution and Redistribution of HIV-1
414 Nucleocapsid Protein in Immature, Mature, and Integrase-Inhibited Virions: a
415 Role for Integrase in Maturation. *J Virol* **2015,** 89, (19), 9765-80.
416 24. Hanne, J.; Gottfert, F.; Schimer, J.; Anders-Osswein, M.; Konvalinka, J.;
417 Engelhardt, J.; Muller, B.; Hell, S. W.; Krausslich, H. G., Stimulated Emission
418 Depletion Nanoscopy Reveals Time-Course of Human Immunodeficiency
419 Virus Proteolytic Maturation. *ACS Nano* **2016,** 10, (9), 8215-22.
420 25. Nagai, T.; Miyawaki, A., A high-throughput method for development of FRET-
421 based indicators for proteolysis. *Biochem Biophys Res Commun* **2004,** 319,
422 (1), 72-7.
423 26. Hubner, W.; Chen, P.; Del Portillo, A.; Liu, Y.; Gordon, R. E.; Chen, B. K.,
424 Sequence of human immunodeficiency virus type 1 (HIV-1) Gag localization
425 and oligomerization monitored with live confocal imaging of a replication-
426 competent, fluorescently tagged HIV-1. *J Virol* **2007,** 81, (22), 12596-607.
427 27. Renner, N.; Kleinpeter, A.; Mallery, D. L.; Albecka, A.; Rifat Faysal, K. M.;
428 Bocking, T.; Saiardi, A.; Freed, E. O.; James, L. C., HIV-1 is dependent on its

429 immature lattice to recruit IP6 for mature capsid assembly. *Nat Struct Mol Biol*
430 **2023,** 30, (3), 370-382.
431 28. Sowd, G. A.; Aiken, C., Correction: Inositol phosphates promote HIV-1
432 assembly and maturation to facilitate viral spread in human CD4+ T cells.
433 *PLoS Pathog* **2021,** 17, (3), e1009389.
434 29. Tabler, C. O.; Wegman, S. J.; Chen, J.; Shroff, H.; Alhusaini, N.; Tilton, J. C.,
435 The HIV-1 Viral Protease Is Activated during Assembly and Budding Prior to
436 Particle Release. *J Virol* **2022,** 96, (9), e0219821.
437 30. Shcherbatova, O.; Grebennikov, D.; Sazonov, I.; Meyerhans, A.; Bocharov, G.,
438 Modeling of the HIV-1 Life Cycle in Productively Infected Cells to Predict
439 Novel Therapeutic Targets. *Pathogens* **2020,** 9, (4).
440 31. Burdick, R. C.; Li, C.; Munshi, M.; Rawson, J. M. O.; Nagashima, K.; Hu, W.
441 S.; Pathak, V. K., HIV-1 uncoats in the nucleus near sites of integration. *Proc*
442 *Natl Acad Sci U S A* **2020,** 117, (10), 5486-5493.
443 32. Li, C.; Burdick, R. C.; Nagashima, K.; Hu, W. S.; Pathak, V. K., HIV-1 cores
444 retain their integrity until minutes before uncoating in the nucleus. *Proc Natl*
445 *Acad Sci U S A* **2021,** 118, (10).
446 33. Freed, E. O., HIV-1 assembly, release and maturation. *Nat Rev Microbiol*
447 **2015,** 13, (8), 484-96.
448 34. Wang, D.; Lu, W.; Li, F., Pharmacological intervention of HIV-1 maturation.
449 *Acta Pharm Sin B* **2015,** 5, (6), 493-9.
450 35. Kleinpeter, A. B.; Freed, E. O., HIV-1 Maturation: Lessons Learned from
451 Inhibitors. *Viruses* **2020,** 12, (9).

452

Figure 1

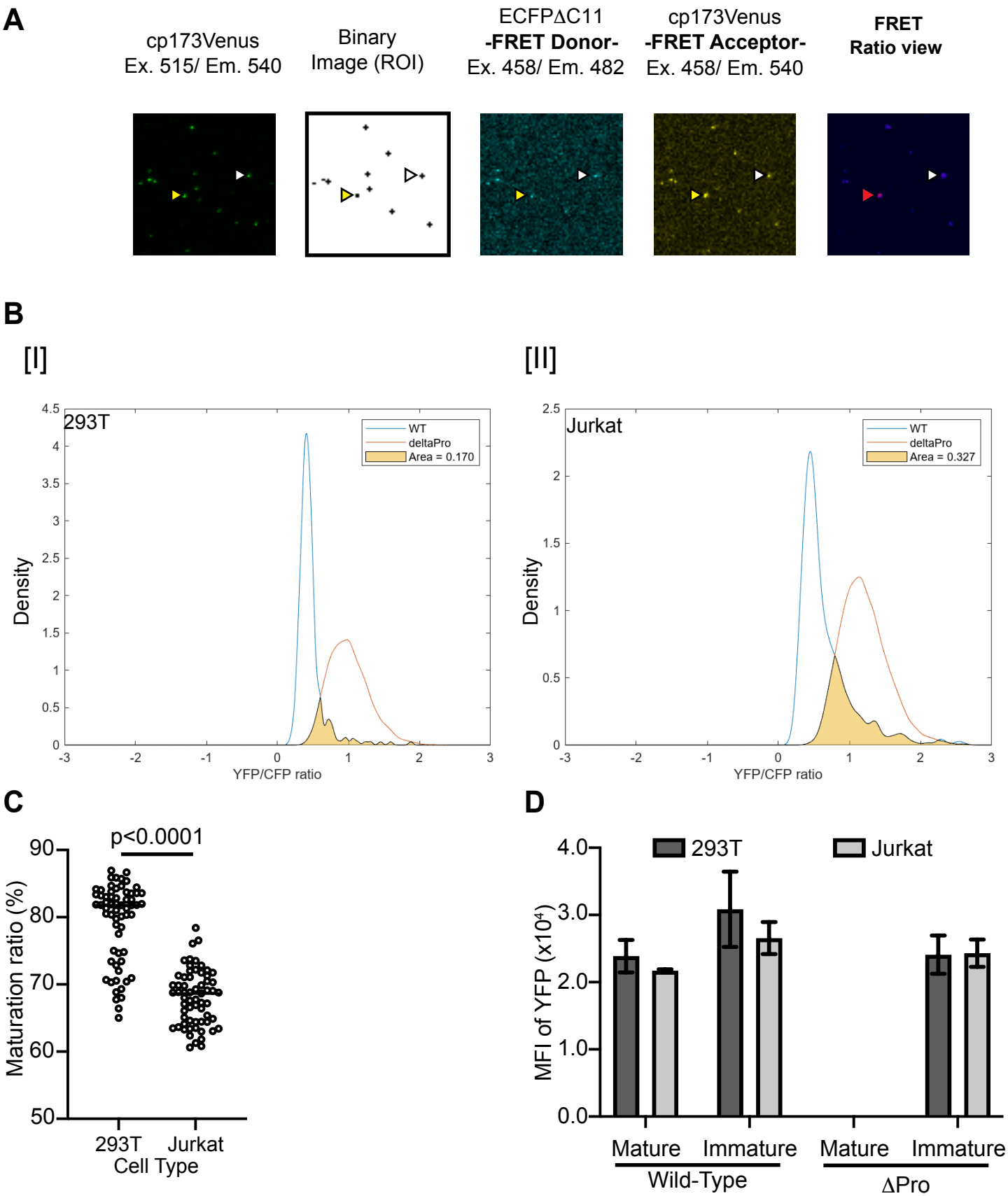
A
cp173Venus
Ex. 515/ Em. 540
Binary
Image (ROI)
ECFPΔC11
-FRET Donor-
Ex. 458/ Em. 482
cp173Venus
-FRET Acceptor-
Ex. 458/ Em. 540
FRET
Ratio view
B
[I]
293T
WT
deltaPro
Area = 0.170
Density
YFP/CFP ratio
[II]
Jurkat
WT
deltaPro
Area = 0.327
Density
YFP/CFP ratio
C
p<0.0001
Maturation ratio (%)
293T
Jurkat
Cell Type
D
293T
Jurkat
MFI of YFP (x10⁴)
Mature
Immature
Wild-Type
Mature
Immature
ΔPro

Figure 2

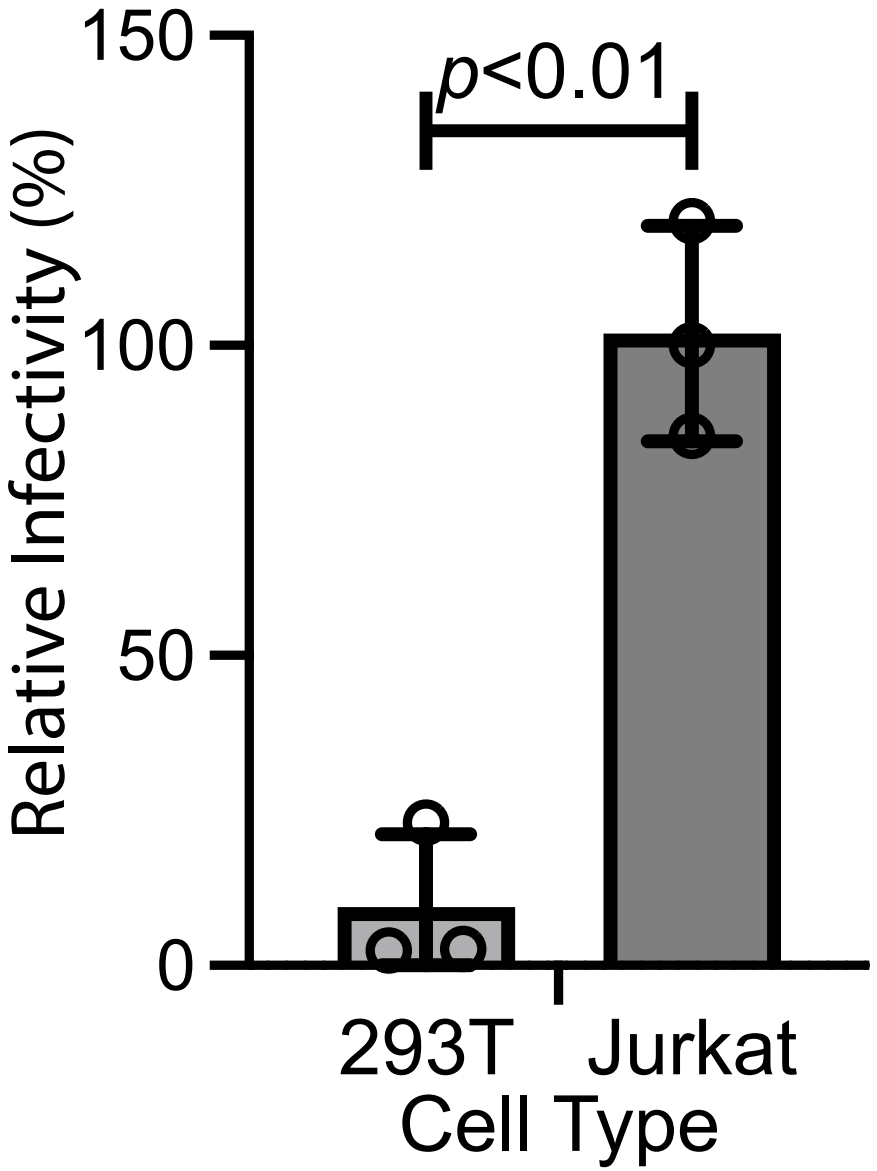
150
100
50
0
Relative Infectivity (%)
p<0.01
293T
Jurkat
Cell Type